American Mineralogist, Volume 64, pages 409–423, 1979

A high-temperature structural study of high albite, monalbite, and the analbite → monalbite phase transition

JOHN K. WINTER, FUJIO P. OKAMURA[1] AND SUBRATA GHOSE

Department of Geological Sciences, University of Washington Seattle, Washington 98195

Abstract

The crystal structures of an albite sample from Tiburon, Marin County, California, annealed at 1080°C for 60 days, were refined from X-ray intensity data collected at 25, 500, 750, 980, and 1040°C to *R* factors of 0.034, 0.036. 0.037, 0.037, and 0.039 for 2443, 1993, 2013, 2016, and 2018 reflections, respectively. The crystal structures of a second albite sample from Amelia, Virginia, annealed at temperatures up to 1110°C for 133 days, were also refined to *R* factors of 0.040 and 0.044 based on 2018 and 430 reflections collected at 980 and 1060°C respectively.

The Tiburon sample failed to attain monoclinic symmetry with respect to either unit-cell dimensions or atomic parameters within the temperature range of study, which is in agreement with an earlier high-temperature investigation by Prewitt *et al.* (1976). Extrapolation of monoclinic indicators based on atomic positions and bond lengths related by pseudo-monoclinic symmetry indicates that monoclinic symmetry would be attained within the temperature range 1050–1075°C for the Tiburon sample and 1105–1110°C for the synthetic albite sample studied by Prewitt *et al.* (1976). The Amelia sample was found to be definitely monoclinic at 980°C. The variable inversion temperatures of these albite samples reflect differences in the degree of Al/Si disorder created by the different annealing times and temperatures. These differences in Al/Si disorder are too slight to be measured by current indirect methods.

The spatial disorder associated with the sodium atom in high albite is attributed to the response of Na to differences in the local Al/Si configurations created by Al/Si disorder. Previous interpretations restricting the number of such configurations to four and assuming isotropic Na quarter-atoms are inadequate. Changes in the electron density distribution about the Na atom as a function of temperature reflect changes in the shape of the aluminosilicate cage surrounding Na as monoclinic symmetry is gradually approached with increasing temperature.

Introduction

Since the first structural analyses of low and high albite were made by Ferguson *et al.* (1958), there have been several unresolved crystallographic problems with regard to the highly anisotropic electron density distribution of the Na atom in both structures, as well as the degree and effects of Al/Si ordering in the tetrahedral positions of the aluminosilicate framework. In addition, considerable controversy has arisen over analbite and the monoclinic → triclinic inversion in "completely" disordered structures. Excellent summaries of the extensive literature devoted to these problems may be found in Ribbe *et al.* (1969), Smith (1974), and Prewitt *et al.* (1976).

In a high-temperature study of low albite, Winter *et al.* (1977) have shown that the anisotropy of the Na atom in low albite is solely the result of thermal vibration. As the Na anisotropy is quite different in the ordered and disordered forms of albite, a knowledge of the properties of low albite is expected to aid the interpretation of a similar series of high-temperature refinements of the more complex high structural state. In addition to the Na behavior, in this paper we discuss the effects of Al/Si disordering on the thermal response of the crystal, as well as on the triclinic → monoclinic transformation.

[1] Present address: National Institute for Researches in Inorganic Materials, Kurakake, Sakura-mura, Niihari-gun, Ibaraki 300-31, Japan.

0003–004X/79/0304–0409$02.00

In a previous high-temperature study of high albite, Prewitt *et al.* (1976) reported that their sample did not attain monoclinic symmetry at or below 1105°C. Prior studies (MacKenzie, 1952; Grundy *et al.*, 1967; Kroll, 1971; Okamura and Ghose, 1975a) indicate transitions at or below 980°C. A full structural analysis of the monoclinic form of albite is desirable in order to verify its existence and to clarify the controls of the inversion itself.

Collection of intensity data and refinement of the crystal structures

The albite crystals, from Tiburon, Marin County, California, had the composition $Ab_{99.75}Or_{0.25}$ and were kindly supplied by B. W. Evans. A sample was sealed in a Pt capsule, annealed at 1080°C for 60 days, and quenched in a stream of air upon removal from the furnace. Clear fragments were selected from the crushed crystals and their crystal perfection verified from transmission Laue photographs. A nearly cubic crystal approximately 200 μm in diameter was mounted on a silica-glass fiber with a cement of ground mullite and sealed in a silica-glass capillary. Details of the microfurnace and the temperature calibration used in the high temperature runs are given by Winter *et al.* (1977). Temperatures are judged to be accurate to within 15°C.

Unit-cell dimensions were determined by least-squares refinement, based on 15 reflections, evenly distributed in reciprocal space between 2 and 40° 2θ (Mo$K\alpha$) measured on an automatic single-crystal diffractometer (Syntex $P\bar{1}$). Two hours were allowed for equilibration at a given temperature. Determinations were made both prior to and following intensity data collection. Agreement between the two data sets was within 2σ, where σ is the standard deviation of the unit-cell dimensions.

Intensities of 1993, 2013, 2016, and 2018 reflections were measured between 3 and 60° 2θ on a Syntex $P\bar{1}$ automated 4-circle diffractometer at 500, 750, 980, and 1040°C, respectively, using Mo$K\alpha$ radiation monochromatized by a graphite crystal. An ω–2θ scan method was used with a variable rate (2°/minute minimum). The data collection at room temperature was performed earlier on a separate crystal from the same sample, whereby 2443 reflections were collected between 2 and 65° 2θ with a 1°/minute minimum scan rate. The sample used for data collection at high temperature was analyzed by the electron microprobe following X-ray analysis and was found to retain the original composition. The intensity data were corrected for Lorentz and polarization effects, but not for absorption or extinction.

Refinements based on space group $C\bar{1}$ were carried out with the full-matrix least-squares program RFINE (Finger, 1969). Atomic scattering factors for Na, Al, Si, and O atoms were taken from Cromer and Mann (1968). Corrections for anomalous dispersion were made according to Cromer and Liberman (1970). The observed structure factors (F_o's) were weighted by $1/\sigma^2(F_o)$, where $\sigma(F_o)$ is the standard deviation of F_o as measured by the counting statistics. Low-intensity reflections with $F_o < 3\sigma(F_o)$ were not included in the refinements. Upon convergence, R factors based on anisotropic temperature factors for unrejected reflections were 0.034, 0.041, 0.038, 0.039, and 0.039 for the 25, 500, 750, 980, and 1040°C analyses respectively. The glass wall of the microfurnace was found to produce a halo of diffuse-scattered X-rays, which may have interfered with the intensity measurements of a few reflections. Due to possible errors resulting from this effect or from secondary extinction, all reflections with $|F_o - F_c| > 5.0$ were excluded from the refinement. Most reflections rejected for this reason had $F_o > F_c$. The effect of this rejection was a slight reduction in R factors and a less than 2σ shift in atomic parameters. Final R factors and the reflection statistics are listed in Table 1.

As will be discussed more fully in later sections, the refined structures were nearly monoclinic at the highest temperature studied, but not exactly so with respect to either cell dimensions or atomic positions. These results agree with the findings of Prewitt *et al.* (1976), and appear to contradict earlier high-temperature precession studies which indicated a transition to the monoclinic form below 980°C.

A fragment of Amelia albite (annealed between 1080 and 1111°C for 133 days by Duba and Piwinskii, 1974), which became monoclinic at 930°C according to a precession study by Okamura and Ghose (1975a), was available. Although unsuitable for structural analysis below the transition temperature due to fine twinning on the albite law, analysis above 930°C should involve a single homogeneous monoclinic phase.

A crystal of the twinned albite was heated at a rate of 50° per hour to 930°C in the microfurnace mounted on the single-crystal diffractometer. A Polaroid Land film cassette was set at $2\theta = 0$ and 35° and full rotation photographs were taken at each 50° interval. In accordance with the findings of Okamura and Ghose (1975a), the separation between the twin-doublets of the observable spots continuously decreased as the temperature was raised, until they merged to single spots at 930°C. In order to avoid any possible effects of thermal hysteresis, the temper-

Table 1. High albite (Tiburon) and monalbite (Amelia): number of reflections measured and R factors

Temp. (°C)	All Refl. R_w	All Refl. R_{unw}	Unrej. R_w	Unrej. R_{unw}	# Refl.	Low I rej.	F_o-F_c>5 rej.
25	0.040*	0.034*	0.040	0.034	2443	428	3
2 Na	0.030*	0.024*	0.030	0.024			
500	0.046	0.045	0.038	0.036	1993	238	25
2 Na	0.043	0.040	0.034	0.031			
750	0.042	0.046	0.038	0.037	2013	296	8
2 Na	0.038	0.042	0.035	0.033			
980	0.042	0.046	0.038	0.037	2016	319	9
2 Na	0.040	0.043	0.035	0.034			
1040	0.060	0.048	0.042	0.039	2018	316	12
2 Na	0.059	0.045	0.037	0.035			
980 M	0.047	0.052	0.039	0.040	1054	182	9
2 Na	0.046	0.050	0.037	0.038			
1060 M	0.051	0.056	0.041	0.044	430	68	7
2 Na	0.050	0.055	0.040	0.043			

* Low intensity reflections edited
M=monoclinic

ature was raised to 980°C. 2018 reflections were measured between 3 and 60° 2θ at this temperature, using a 2°/minute minimum scan rate.

The intensity data were converted to structure factors. As a test for monoclinic intensity distribution, calculations were performed of both weighted and unweighted R^* factors for all the observed pairs F_{hkl} and $F_{h\bar{k}l}$, defined by:

$$R^* = \frac{\Sigma(|F_{hkl}| - |F_{h\bar{k}l}|)}{\Sigma|F_{hkl}|}$$

and

$$wR^* = \frac{\Sigma[w_{hkl}(|F_{hkl}| - |F_{h\bar{k}l}|)]}{\Sigma|(w_{hkl}F_{hkl})|}$$

where

$$w = \frac{(\sigma F_{hkl} + \sigma F_{h\bar{k}l})}{2}$$

The values of $R^* = 0.045$ and $wR^* = 0.041$ are significantly small as to indicate monoclinic symmetry within average fluctuations of F_o due to counting errors.

Refinement procedures identical to those discussed above, but including the low-intensity reflections, resulted in weighted and unweighted R factors of 0.040 and 0.049 respectively for space group $C\bar{1}$. As the cell dimensions and all the atomic parameters, including anisotropic temperature factors, clearly indicated monoclinic symmetry, the space group was switched from $C\bar{1}$ to $C2/m$. Refinement in the monoclinic space group was initiated, using 1054 averaged reflections where $F_{hkl} = (F_{hkl} + F_{h\bar{k}l})/2$. Two cycles of anisotropic refinement were required for convergence, resulting in weighted and unweighted R factors of 0.039 and 0.049. Final R factors, excluding F_o's $< 3\sigma(F_o)$, are listed in Table 1.

The collection of intensity data based on a monoclinic unit cell was begun on the same sample at 1060°C, but was discontinued after collecting 430 reflections because of failure of the furnace after prolonged use at high temperatures. Results of the refinement based on the partial data set, although subject to substantially greater uncertainties, are included with the other data in the tables. A preliminary report on the 980°C monalbite refinement has already been published (Okamura and Ghose, 1975b).

Cell dimensions, atomic parameters, and thermal ellipsoids are listed in Tables 2, 4, and 5 respectively. Interatomic distances and angles are given in Tables 6 and 7. Observed and calculated structure factors are compared in Table 8[2].

[2] To obtain a copy of this table, order Document AM-79-092 from the Business Office, Mineralogical Society of America, 1909 K Street, N.W., Washington, D.C. 20006. Please remit $1.00 in advance for the microfiche.

Table 2. High albite (Tiburon) and monalbite (Amelia): cell dimensions as a function of temperature (with standard deviations in parentheses)

	25°C	500°C	750°C	980°C	1000°C	1020°C	1040°C	1062°C	1080°C	980°C M*	1060°C M*
a (Å)	8.161(1)	8.208(2)	8.234(1)	8.259(1)	8.263(2)	8.266(2)	8.270(2)	8.272(2)	8.276(2)	8.274(5)	8.297(5)
b (Å)	12.875(2)	12.934(4)	12.955(4)	12.975(3)	12.976(4)	12.975(4)	12.978(4)	12.981(4)	12.982(4)	12.991(6)	12.994(6)
c (Å)	7.110(1)	7.134(2)	7.143(2)	7.151(2)	7.152(2)	7.153(2)	7.154(2)	7.155(2)	7.154(2)	7.144(4)	7.144(5)
α (°)	93.53(1)	92.65(2)	92.00(2)	90.81(2)	90.58(2)	90.37(2)	90.22(2)	90.17(2)	90.15(2)	90.06(4)	90.03(4)
β (°)	116.46(1)	116.25(2)	116.17(2)	116.08(2)	116.08(2)	116.07(2)	116.05(2)	116.04(2)	116.02(2)	116.13(4)	116.01(4)
γ (°)	90.24(1)	90.12(2)	90.06(2)	89.99(2)	89.98(2)	89.96(2)	89.96(2)	89.96(2)	89.96(2)	90.05(4)	89.99(4)
V (Å^3)	669.8(2)	678.4(3)	683.3(3)	688.2(3)	688.8(3)	689.1(3)	689.9(3)	690.4(4)	690.7(3)	689.4(6)	692.2(6)

*M=monoclinic

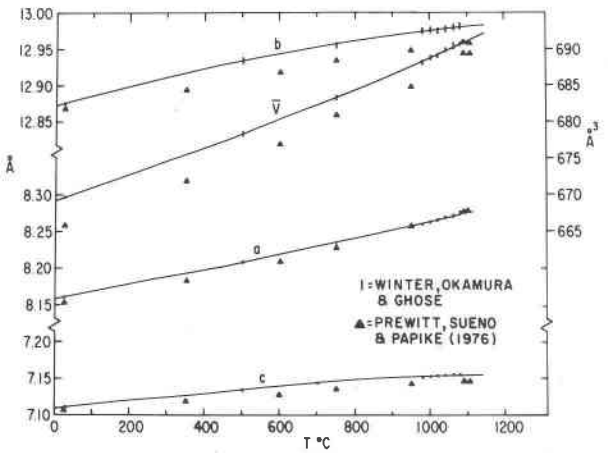

Fig. 1. Unit-cell dimensions and volume of high albite *vs.* temperature. Solid triangles represent the data of Prewitt *et al.* (1976). Line symbols represent the data of the present study. Length of the lines represents ±one standard deviation.

Results and discussion

Unit-cell dimensions and ellipsoids of thermal expansion

Axial dimensions, unit-cell volume, and interaxial angles at various temperatures are shown in Figures 1 and 2. All cell dimensions show an increase as temperature is raised. The interaxial angles α and γ approach 90° with increasing temperature, α showing a higher rate of change because it begins farther from the 90° angle. Note that α approaches 90° asymptotically above 1000°C, while γ actually crosses the 90° point and becomes acute.

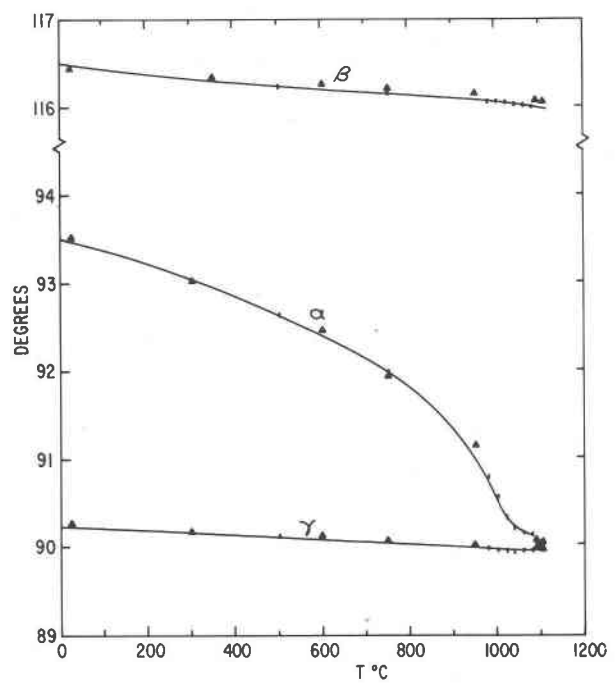

Fig. 2. Unit-cell angles of high albite *vs.* temperature. Symbols are the same as in Fig. 1.

Table 3. Tiburon albite: principal strain components of thermal expansion for high albite and of the high-to-low albite transformations (with standard deviations in parentheses)

Variable Range	Principal Strian Components per 1°C x10^{-5}	Orientation of Principal Axes: Angle (degrees) with respect to: +*a*	+*b*	+*c*
25→500°C	3.22(6)	75(1)	51(1)	60(1)
	1.08(4)	16(1)	104(1)	122(1)
	-0.79(7)	84(1)	43(1)	134(1)
25→750°C	3.37(5)	77(1)	50(1)	59(1)
	1.10(3)	14(1)	102(1)	122(1)
	-1.15(5)	86(1)	43(1)	133(1)
25→980°C	4.05(4)	79(1)	50(1)	58(1)
	1.14(2)	11(1)	100(1)	121(1)
	-1.91(3)	87(1)	42(1)	132(1)
25→1040°C	4.46(4)	80(1)	50(1)	57(1)
	1.18(2)	10(1)	99(1)	121(1)
	-2.33(4)	87(1)	42(1)	132(1)
25→1080°C	4.39(4)	80(1)	50(1)	57(1)
	1.19(2)	11(1)	99(1)	121(1)
	-2.28(3)	87(1)	42(1)	132(1)
High→Low	1.75*	42(1)	49(1)	113(1)
	0.67*	94(1)	84(1)	24(1)
	-2.68*	131(1)	42(1)	82(1)

*values x 10^{-2} for High→Low transition

The principal directions of thermal expansion in triclinic feldspars do not coincide with the principal unit-cell directions. Therefore, thermal expansion ellipsoids have been computed between 25° and 500, 750, 980, 1040, and 1080°C respectively, using the program STRAIN (Ohashi and Finger, 1973). The results are given in Table 3 and Figure 3; the latter also includes the data for low albite (Winter *et al.*, 1977). The high and low albite data are comparable, and agree with previous studies on other feldspars (Ohashi and Finger, 1973; Willaime *et al.*, 1974). The magnitude and orientation of the thermal expansion ellipsoid for low albite have been discussed by Winter *et al.* (1977). They suggested that the thermal response of low albite is the result of three interacting factors: (1) the greater flexibility of the structure along the axes of the elastic aluminosilicate double crankshafts (the *a* cell direction), (2) restrictions imposed on this flexibility by the linking of adjacent crankshafts along *c* by T–O_{A1}–T bonds, and (3) an approach toward monoclinic geometry.

The slight differences in the orientation of the thermal strain ellipsoids between high albite and low albite must result from changes in the aluminosilicate

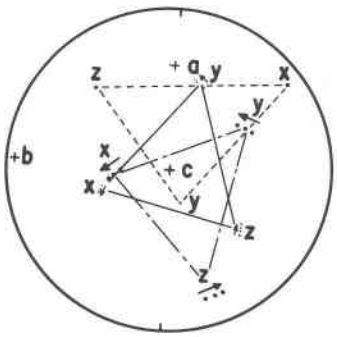

Fig. 3. Stereographic projection of the minimum (x), intermediate (y), and maximum (z) axes of the thermal expansion ellipsoids for: (1) low albite (connected by dot-dash line) at 25→500°, 25→750°, and 25→970°C respectively in the direction of the arrows; (2) high albite (solid line) at 25→500°, 25→750°, 25→980°, and 25→1040°C respectively in the direction of the arrows; and (3) the high→low albite transformation at 25°C (dashed line). Cell axes of low albite are included.

framework caused by Al/Si disordering. A calculation similar to those of the thermal expansion ellipsoids was made for high to low albite. In order to isolate the strain effects of ordering from those of thermal origin, the high and low forms of albite at 25°C were compared using the STRAIN program. The results are included in Table 3 and Figure 3. The structural changes involved in the high to low transition were treated by Stewart and Ribbe (1969). Since the AlO_4 tetrahedron is larger than the SiO_4 tetrahedron, they assumed that the T–O–T–O–T path with the highest density of $T_1(o)$ positions would show the greatest expansion, since Al concentrates in this position with progressive Al/Si ordering. This seems a well-reasoned approach; however, without calculating a strain ellipsoid, they were confined to dealing

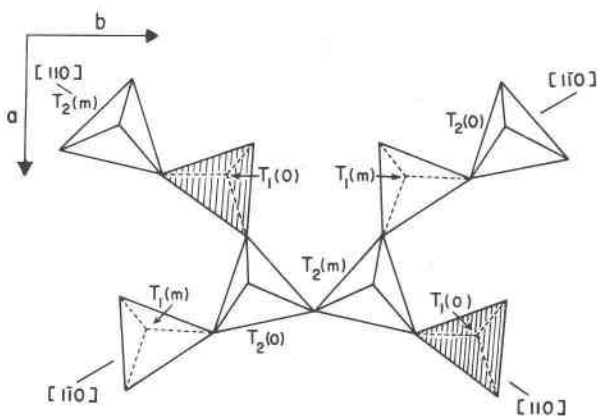

Fig. 4. (001) section of high albite showing direction [110] with $[T_1(o)/\Sigma T] = 1/3$ and direction [1$\bar{1}$0] with $[T_1(o)/\Sigma T] = 0$.

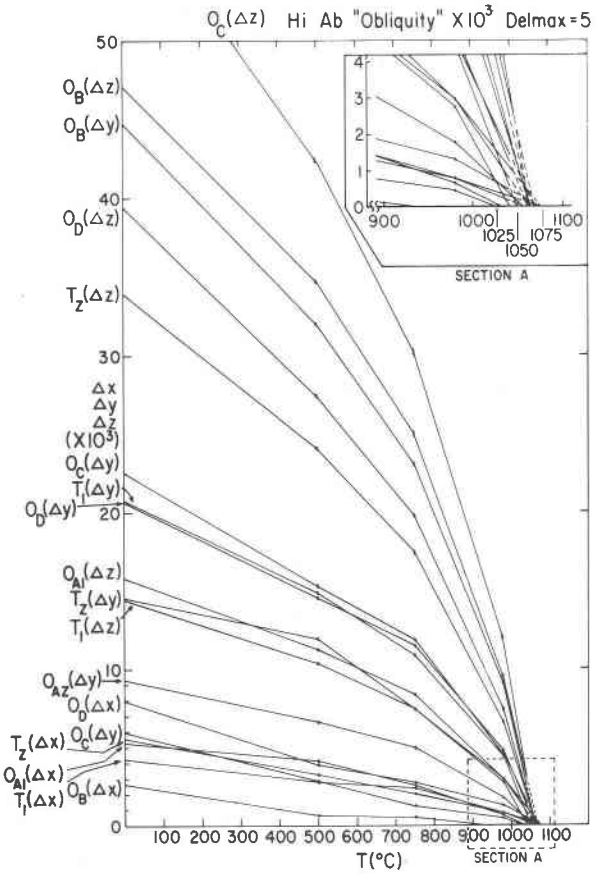

Fig. 5. "Obliquity" *vs.* temperature for high albite extrapolated to the monoclinic value. See text for definitions.

exclusively with axial directions. The thermal ellipsoids show that the direction of maximum expansion is not the c cell dimension but [110], and the direction of minimum expansion (negative in this case) is [1$\bar{1}$0]. The tetrahedral configuration in high albite within the ab plane is shown in Figure 4. The [110] direction represents a path $T_2(m)$–$T_1(o)$–$T_2(o)$–$T_2(m)$–$T_1(o)$– with the ratio of $T_1(o)/\Sigma T = 1/3$, the same as for the c direction; along the [1$\bar{1}$0] direction $T_1(o)/\Sigma T = 0$. Thus, as Al concentrates in $T_1(o)$, the [1$\bar{1}$0] direction will contract as the Al/Si ratio decreases from 0.25 to 0, whereas the [110] direction will expand as this ratio increases from 0.25 to 0.33 (Kroll, 1973). This coplanar combination results in the large observed decrease in γ as high albite reverts to low albite and causes the [110] direction to expand more than c. In summary, the isothermal disordering transition from low to high albite causes changes principally in γ, whereas the heating of a disordered high albite causes changes principally in α. Both changes are of the same magnitude (~3°) and approach a value of 90°.

Table 4a. High albite (Tiburon): atomic positional parameters and temperature factors as a function of temperature (with standard deviations in parentheses)

		25°C	500°C	750°C	980°C	1040°C
Na	x	.2737(2)	.2759(3)	.2774(3)	.2789(3)	.2794(4)
	y	.0075(2)	.0033(3)	.0024(3)	.0007(3)	1.0000(3)
	z	.1332(3)	.1375(5)	.1378(5)	.1386(5)	.1378(5)
	β_{11}	.0072(3)	.0147(4)	.0189(4)	.0227(5)	.0243(6)
	β_{22}	.0182(3)	.0215(4)	.0240(4)	.0258(4)	.0267(5)
	β_{33}	.0425(7)	.0589(11)	.0642(11)	.0731(13)	.0718(13)
	β_{12}	.0016(2)	.0014(3)	.0011(3)	.0005(4)	-.0003(4)
	β_{13}	.0011(3)	.0057(5)	.0085(6)	.0109(7)	.0114(7)
	β_{23}	-.0207(4)	-.0176(6)	-.0133(5)	-.0055(6)	-.0009(6)
$T_1(o)$	x	.0090(1)	.0087(1)	.0087(1)	.0082(1)	.0081(1)
	y	.1649(1)	.1690(1)	.1718(1)	.1757(1)	.1776(1)
	z	.2147(1)	.2173(1)	.2191(1)	.2217(1)	.2239(1)
	β_{11}	.0043(1)	.0077(1)	.0094(1)	.0108(1)	.0112(1)
	β_{22}	.0014(1)	.0026(1)	.0032(1)	.0039(1)	.0042(1)
	β_{33}	.0048(1)	.0081(2)	.0099(1)	.0116(2)	.0120(2)
	β_{12}	-.0004(1)	-.0005(1)	-.0007(1)	-.0008(1)	-.0009(1)
	β_{13}	.0021(1)	.0036(1)	.0044(1)	.0051(1)	.0054(1)
	β_{23}	.0001(1)	.0003(1)	.0002(1)	.0001(1)	-.0001(1)
$T_1(m)$	x	.0048(1)	.0059(1)	.0065(1)	.0074(1)	.0078(1)
	y	.8146(1)	.8161(1)	.8173(1)	.8199(1)	.8212(1)
	z	.2289(1)	.2277(1)	.2266(1)	.2245(1)	.2236(1)
	β_{11}	.0041(1)	.0077(1)	.0093(1)	.0108(1)	.0112(1)
	β_{22}	.0015(1)	.0026(1)	.0032(1)	.0039(1)	.0042(1)
	β_{33}	.0047(1)	.0079(2)	.0098(1)	.0116(2)	.0121(2)
	β_{12}	.0004(1)	.0010(1)	.0011(1)	.0012(1)	.0012(2)
	β_{13}	.0020(1)	.0036(1)	.0044(1)	.0052(1)	.0054(1)
	β_{23}	.0003(1)	.0006(1)	.0006(1)	.0004(1)	.0003(1)
$T_2(o)$	x	.6904(1)	.6929(1)	.6941(1)	.6952(1)	.6955(1)
	y	.1080(1)	.1105(1)	.1121(1)	.1146(1)	.1158(1)
	z	.3202(1)	.3272(1)	.3316(1)	.3382(1)	.3409(1)
	β_{11}	.0038(1)	.0068(1)	.0083(1)	.0098(1)	.0101(1)
	β_{22}	.0012(1)	.0021(1)	.0026(1)	.0031(1)	.0035(1)
	β_{33}	.0059(1)	.0100(2)	.0127(2)	.0150(2)	.0155(2)
	β_{12}	-.0001(1)	.0000(1)	-.0002(1)	-.0003(1)	-.0003(1)
	β_{13}	.0018(1)	.0029(1)	.0037(1)	.0045(1)	.0046(1)
	β_{23}	.0002(1)	.0004(1)	.0004(1)	.0002(1)	.0000(1)
$T_2(m)$	x	.6849(1)	.6896(1)	.6920(1)	.6944(1)	.6953(1)
	y	.8776(1)	.8793(1)	.8804(1)	.8824(1)	.8834(1)
	z	.3537(1)	.3513(1)	.3491(1)	.3448(1)	.3427(1)
	β_{11}	.0039(1)	.0070(1)	.0084(1)	.0098(1)	.0102(1)
	β_{22}	.0011(1)	.0021(1)	.0025(1)	.0032(1)	.0035(1)
	β_{33}	.0059(1)	.0104(2)	.0128(2)	.0148(2)	.0154(2)
	β_{12}	.0001(1)	.0004(1)	.0006(1)	.0006(1)	.0006(1)
	β_{13}	.0019(1)	.0034(1)	.0041(1)	.0047(1)	.0048(1)
	β_{23}	.0003(1)	.0006(1)	.0006(1)	.0005(4)	.0003(4)
O_{A1}	x	.0053(3)	.0042(3)	.0026(3)	.0007(4)	.9999(4)
	y	.1348(1)	.1372(2)	.1383(2)	.1390(2)	.1389(2)
	z	.9844(3)	.9887(3)	.9916(3)	.9970(4)	.9989(4)
	β_{11}	.0107(4)	.0194(5)	.0232(6)	.0266(6)	.0280(8)
	β_{22}	.0025(1)	.0047(1)	.0059(2)	.0072(2)	.0075(2)
	β_{33}	.0085(4)	.0130(5)	.0149(5)	.0172(6)	.0174(6)
	β_{12}	.0002(2)	.0006(2)	.0004(2)	.0005(3)	.0000(2)
	β_{13}	.0055(3)	.0091(4)	.0110(5)	.0120(5)	.0128(6)
	β_{23}	.0005(2)	.0010(2)	.0010(2)	.0004(3)	.0002(3)
$O_B(o)$	x	.8214(2)	.8218(3)	.8231(3)	.8231(3)	.8236(4)
	y	.1086(1)	.1166(2)	.1223(2)	.1302(2)	.1334(3)
	z	.1991(3)	.2058(4)	.2123(4)	.2199(5)	.2231(5)
	β_{11}	.0078(3)	.0134(4)	.0157(5)	.0178(5)	.0184(6)
	β_{22}	.0025(1)	.0054(1)	.0068(2)	.0087(2)	.0097(3)
	β_{33}	.0132(5)	.0226(6)	.0280(7)	.0331(8)	.0349(9)
	β_{12}	-.0009(1)	-.0020(2)	-.0023(2)	-.0029(3)	-.0030(3)
	β_{13}	.0061(3)	.0106(4)	.0126(5)	.0146(6)	.0154(7)
	β_{23}	-.0004(2)	-.0003(2)	.0003(3)	-.0006(3)	-.0007(4)
$O_B(m)$	x	.8188(3)	.8211(1)	.8225(3)	.8233(1)	.8237(1)
	y	.8472(2)	.8514(2)	.8546(2)	.8608(3)	.8641(3)
	z	.2456(3)	.2405(4)	.2373(4)	.2293(5)	.2261(5)
	β_{11}	.0073(3)	.0139(4)	.0166(5)	.0182(6)	.0186(6)
	β_{22}	.0035(1)	.0064(2)	.0079(2)	.0093(2)	.0096(3)
	β_{33}	.0143(5)	.0262(7)	.0299(8)	.0339(7)	.0343(9)
	β_{12}	.0008(1)	.0024(3)	.0029(2)	.0034(3)	.0036(3)
	β_{13}	.0065(3)	.0120(5)	.0143(5)	.0155(6)	.0158(6)
	β_{23}	-.0002(2)	.0002(3)	.0003(3)	-.0003(3)	.0001(4)
$O_C(o)$	x	.0159(2)	.0199(3)	.0220(3)	.0243(3)	.0248(3)
	y	.2906(1)	.2946(2)	.2972(2)	.3012(2)	.3030(2)
	z	.2773(3)	.2715(3)	.2667(4)	.2596(4)	.2556(4)
	β_{11}	.0065(3)	.0120(4)	.0139(4)	.0161(5)	.0166(5)
	β_{22}	.0021(1)	.0033(1)	.0040(1)	.0046(1)	.0049(2)
	β_{33}	.0111(4)	.0204(6)	.0255(6)	.0294(7)	.0300(8)
	β_{12}	-.0003(1)	-.0007(2)	-.0011(2)	-.0012(2)	-.0017(2)
	β_{13}	.0036(3)	.0065(4)	.0075(4)	.0079(5)	.0073(5)
	β_{23}	-.0002(2)	-.0005(2)	-.0008(2)	-.0008(2)	-.0012(3)
$O_C(m)$	x	.0217(2)	.0228(3)	.0233(3)	.0248(3)	.0246(3)
	y	.6872(1)	.6896(2)	.6909(2)	.6943(2)	.6956(2)
	z	.2184(3)	.2292(3)	.2365(4)	.2477(4)	.2524(4)
	β_{11}	.0067(3)	.0120(4)	.0139(4)	.0160(5)	.0170(5)
	β_{22}	.0021(1)	.0033(1)	.0039(1)	.0046(1)	.0048(2)
	β_{33}	.0099(4)	.0190(6)	.0239(6)	.0294(7)	.0299(8)
	β_{12}	.0008(1)	.0014(2)	.0016(2)	.0018(2)	.0019(2)
	β_{13}	.0020(3)	.0039(4)	.0050(4)	.0067(5)	.0071(5)
	β_{23}	.0002(2)	.0009(2)	.0011(2)	.0010(2)	.0012(3)
$O_D(o)$	x	.1962(2)	.1925(3)	.1913(3)	.1894(3)	.1887(4)
	y	.1122(1)	.1151(2)	.1174(2)	.1211(2)	.1226(2)
	z	.3879(3)	.3929(3)	.3962(3)	.4022(4)	.4044(4)
	β_{11}	.0070(3)	.0133(4)	.0158(4)	.0182(6)	.0193(6)
	β_{22}	.0022(1)	.0046(1)	.0060(2)	.0074(2)	.0078(2)
	β_{33}	.0078(4)	.0126(5)	.0148(5)	.0177(6)	.0183(6)
	β_{12}	.0006(1)	.0015(2)	.0018(2)	.0020(2)	.0018(4)
	β_{13}	.0018(3)	.0021(3)	.0022(4)	.0023(4)	.0022(4)
	β_{23}	.0006(2)	.0014(2)	.0017(2)	.0016(3)	.0017(3)
$O_D(m)$	x	.1884(2)	.1886(3)	.1885(3)	.1881(3)	.1882(4)
	y	.8674(1)	.8695(2)	.8710(2)	.8741(2)	.8762(2)
	z	.4267(3)	.4203(3)	.4160(3)	.4095(4)	.4063(4)
	β_{11}	.0070(3)	.0135(4)	.0160(5)	.0188(6)	.0189(6)
	β_{22}	.0026(1)	.0051(1)	.0063(2)	.0074(2)	.0079(2)
	β_{33}	.0083(4)	.0129(5)	.0153(5)	.0179(6)	.0184(6)
	β_{12}	-.0004(1)	-.0007(2)	-.0010(2)	-.0018(2)	-.0018(3)
	β_{13}	.0007(3)	.0008(4)	.0012(4)	.0012(4)	.0017(5)
	β_{23}	-.0005(2)	-.0008(2)	-.0007(2)	-.0016(3)	-.0018(3)

Atomic positional parameters as a function of temperature

Atomic positions change smoothly toward monoclinic symmetry in high albite as temperature is raised. The results of a simple calculation of "obliquity" are given in Table 9 and Figure 5. "Obliquity" values (Δx, Δy, and Δz) are defined as follows: Δx is the difference in the x coordinates of atom pairs related by pseudo-monoclinic mirror symmetry, *i.e.* $|^{x}O_B(o) - {}^{x}O_B(m)|$. Similarly, $\Delta z = |z_o - z_m|$ and $\Delta y = |(1 - y_o) - y_m|$. A negative value in Table 5 indicates that the calculated value has passed through zero with increasing temperature. "Obliquity" thus defined gives a direct measure of deviations from

Table 4a. (continued)

		25°C	500°C	750°C	980°C	1040°C
O_{A2}	x	.5917(2)	.5978(3)	.6013(3)	.6051(3)	.6061(3)
	y	.9908(1)	.9933(1)	.9949(1)	.9982(2)	.9996(2)
	z	.2787(3)	.2812(3)	.2823(3)	.2843(4)	.2844(4)
	β_{11}	.0056(3)	.0101(3)	.0115(4)	.0134(4)	.0138(5)
	β_{22}	.0017(1)	.0026(1)	.0031(1)	.0036(1)	.0040(1)
	β_{33}	.0102(4)	.0178(5)	.0210(5)	.0243(6)	.0257(7)
	β_{12}	-.0001(1)	.0003(1)	.0002(2)	.0002(2)	.0002(2)
	β_{13}	.0025(3)	.0043(3)	.0046(4)	.0046(4)	.0052(5)
	β_{23}	.0008(2)	.0012(2)	.0010(2)	.0005(2)	.0003(2)
Na_1*	x	.2716(4)	.2755(9)	.2786(11)	.2730(15)	.2715(15)
	y	.9852(3)	.9821(5)	.9822(7)	.9827(9)	.9824(9)
	z	.1639(5)	.1673(12)	.1659(14)	.1523(23)	.1436(25)
	β_{11}	.0086(4)	.0171(8)	.0205(10)	.0277(13)	.0285(14)
	β_{22}	.0086(3)	.0132(6)	.0155(8)	.0176(9)	.0182(10)
	β_{33}	.0240(10)	.0421(21)	.0478(25)	.0654(30)	.0652(27)
	β_{12}	-.0031(3)	-.0041(6)	-.0042(8)	-.0092(9)	-.0107(9)
	β_{13}	.0076(5)	.0110(11)	.0121(14)	.0178(15)	.0153(14)
	β_{23}	-.0070(4)	-.0052(8)	-.0017(9)	-.0036(13)	-.0025(13)
Na_2*	x	.2785(4)	.2795(8)	.2801(11)	.2874(11)	.2899(12)
	y	.0264(2)	.0222(5)	.0220(6)	.0211(8)	.0200(9)
	z	.1068(5)	.1112(11)	.1113(14)	.1252(24)	.1329(26)
	β_{11}	.0063(4)	.0134(7)	.0187(10)	.0176(12)	.0181(12)
	β_{22}	.0057(2)	.0105(4)	.0139(7)	.0179(10)	.0172(10)
	β_{33}	.0198(8)	.0376(17)	.0453(22)	.0733(29)	.0834(32)
	β_{12}	.0017(2)	.0035(5)	.0052(7)	.0027(9)	.0011(9)
	β_{13}	.0017(4)	.0050(8)	.0069(10)	.0103(15)	.0112(17)
	β_{23}	-.0035(3)	-.0023(6)	.0013(8)	.0043(14)	.0050(16)

* 2 Na model; T and O parameters are virtually the same as given above.

monoclinic symmetry on the atomic level. Extrapolation of "obliquity" values with temperature for the Tiburon sample indicates convergence to monoclinic symmetry in the range 1050–1075°C (Fig. 5). Average "obliquity" values of 20.1, 14.5, 10.6, 4.1, and 1.1 ($\times 10^{-3}$) were calculated for 25, 500, 750, 980, and 1040°C respectively. A plot of Na–O bond distances (*cf.* Prewitt *et al.*, 1976) indicates that pseudo-mirror equivalent Na–O bond distances become equal at extrapolated temperatures between 1057 and 1063°C (Fig. 6). The magnitude of an individual Na–O bond length does not necessarily determine the degree of change in that bond length as temperature is raised (Fig. 6). The tendency toward monoclinic symmetry clearly dominates changes in the Na–O bond lengths. This fact supports the contention of Winter *et al.* (1977) that Na is relatively passive within the aluminosilicate cage.

Calculations of "obliquity" as a function of temperature for the low albite data of Winter *et al.* (1977) also show a progressive shift toward monoclinic symmetry at high temperatures. However, the magnitude of this change is generally less than one-quarter of that for high albite. Average obliquity equals 23.2, 20.6, 18.9, and 17.0 ($\times 10^{-3}$) at 25, 500, 750, and 970°C respectively. This shift toward symmetrically monoclinic atomic positions in both high and low albite is a non-quenchable, displacive change and, in conjunction with the quenchable, diffusive Al/Si disorder, constitutes the thermal response of albite to increased temperature.

At a given temperature, there is only one equilibrium value for both Al/Si order and "obliquity." Our experiments deal with a frozen-in value of Al/Si order and thus are non-equilibrium. The Al/Si distribution in analbite is topochemically monoclinic; hence, the obliquity parameter can reach zero at elevated temperatures, where the distortion of the aluminosilicate cage about the small Na atom is overcome. In low albite the Al/Si distribution is topochemically triclinic, and the approach of obliquity to zero at high temperatures is greatly inhibited. This suggests that

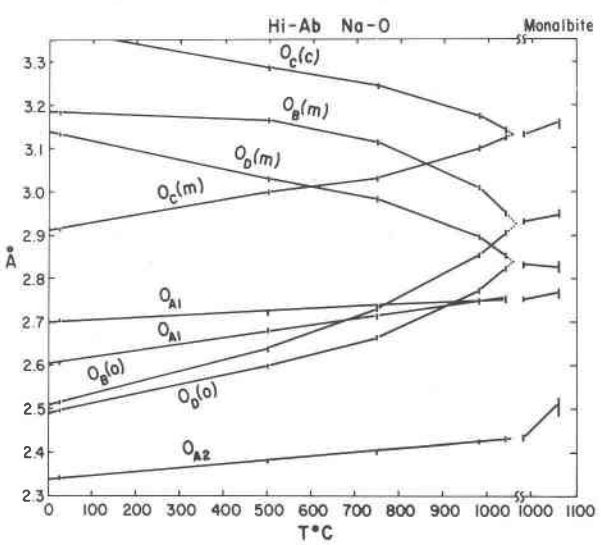

Fig. 6. Na–O bond distances *vs.* temperature for high albite and monalbite.

Table 4b. Monalbite (Amelia): atomic positional parameters and anisotropic temperature factors *vs.* temperature (with standard deviations in parentheses)

		980°C	1060°C			980°C	1060°C
Na	x	0.2789(6)	0.2775(19)	O_B	x	0.8233(4)	0.8227(16)
	y	0.0000	0.0000		y	0.1350(3)	0.1366(5)
	z	0.1378(9)	0.1385(16)		z	0.2252(5)	0.2246(10)
	β_{11}	0.0244(9)	0.0518(101)		β_{11}	0.0183(5)	0.0235(74)
	β_{22}	0.0261(9)	0.0275(13)		β_{22}	0.0101(3)	0.0098(5)
	β_{33}	0.0775(2)	0.0787(39)		β_{33}	0.0371(9)	0.0423(19)
	β_{12}	0.0000	0.0000		β_{12}	-0.0036(3)	-0.0063(12)
	β_{13}	0.0112(12)	0.0077(44)		β_{13}	0.0163(6)	0.0174(25)
	β_{23}	0.0000	0.0000		β_{23}	0.0002(4)	0.0015(7)
T_1	x	0.0081(1)	0.0084(6)	O_C	x	0.0257(4)	0.0294(15)
	y	0.1784(1)	0.1787(1)		y	0.3044(2)	0.3049(3)
	z	0.2233(1)	0.2236(2)		z	0.2535(5)	0.2537(8)
	β_{11}	0.0113(1)	0.0219(21)		β_{11}	0.0176(5)	0.0362(57)
	β_{22}	0.0042(1)	0.0042(7)		β_{22}	0.0048(1)	0.0049(2)
	β_{33}	0.0127(1)	0.0148(3)		β_{33}	0.0330(8)	0.0348(15)
	β_{12}	-0.0011(1)	-0.0008(2)		β_{12}	-0.0019(2)	-0.0017(7)
	β_{13}	0.0053(1)	0.0061(5)		β_{13}	0.0085(5)	0.0109(19)
	β_{23}	-0.0002(1)	-0.0002(1)		β_{23}	-0.0013(3)	-0.0012(4)
T_2	x	0.6959(1)	0.6975(5)	O_D	x	0.1891(4)	0.1873(13)
	y	0.1163(1)	0.1166(1)		y	0.1229(3)	0.1233(4)
	z	0.3420(1)	0.3421(3)		z	0.4049(4)	0.4044(7)
	β_{11}	0.0104(1)	0.0194(17)		β_{11}	0.0193(5)	0.0256(52)
	β_{22}	0.0035(1)	0.0034(6)		β_{22}	0.0085(2)	0.0085(3)
	β_{33}	0.0159(2)	0.0195(3)		β_{33}	0.0184(5)	0.0231(10)
	β_{12}	-0.0005(1)	-0.0007(2)		β_{12}	0.0024(3)	0.0018(8)
	β_{13}	0.0047(1)	0.0053(5)		β_{13}	0.0021(4)	0.0028(16)
	β_{23}	-0.0002(1)	-0.0003(1)		β_{23}	0.0024(3)	0.0023(5)
O_{A1}	x	0.0000	0.0000	Na_1^*	x	0.2810(8)	0.2806(17)
	y	0.1393(3)	0.1411(5)		y	0.9791(11)	0.9830(29)
	z	0.0000	0.0000		z	0.1399(11)	0.1408(15)
	β_{11}	0.0286(10)	0.0305(68)		β_{11}	0.0251(10)	0.0539(77)
	β_{22}	0.0072(3)	0.0076(4)		β_{22}	0.0150(14)	0.0226(31)
	β_{33}	0.0180(8)	0.0218(14)		β_{33}	0.0767(26)	0.0795(34)
	β_{12}	0.0000	0.0000		β_{12}	-0.0050(10)	-0.0131(36)
	β_{13}	0.0123(7)	0.0180(22)		β_{13}	0.0122(14)	0.0100(36)
	β_{23}	0.0000	0.0000		β_{23}	-0.0028(13)	-0.0091(28)
O_{A2}	x	0.6063(5)	0.6126(17)				
	y	0.0000	0.0000				
	z	0.2835(6)	0.2852(10)				
	β_{11}	0.0142(6)	0.0281(62)				
	β_{22}	0.0038(15)	0.0038(2)				
	β_{33}	0.0262(9)	0.0315(18)				
	β_{12}	0.0000	0.0000				
	β_{13}	0.0052(6)	0.0092(22)				
	β_{23}	0.0000	0.0000				

* 2 Na model; the T and O parameters are virtually the same as given above.

Table 5. High albite and monalbite: anisotropic displacement ellipsoid, axial lengths (A) and isotropic equivalent temperature factors (A^2) as a function of temperature

		25°C	500°C	750°C	980°C	1040°C	980°C M	1060°C M
Na	R_1	0.137	0.200	0.228	0.251	0.260	0.261	0.346
	R_2	0.167	0.271	0.327	0.401	0.415	0.433	0.485
	R_3	0.498	0.513	0.507	0.485	0.477	0.473	0.494
	B	7.75(8)	9.9(1)	11.0(1)	12.1(1)	12.3(1)	12.0(2)	15.8(8)
$T_1(o)$	R_1	0.095	0.127	0.140	0.153	0.156	0.162	0.175
	R_2	0.100	0.137	0.151	0.165	0.169	0.167	0.188
	R_3	0.119	0.158	0.175	0.191	0.196	0.199	0.261
	B	0.87(1)	1.57(1)	1.92(1)	2.30(1)	2.41(2)	2.47(1)	3.5(2)
$T_1(m)$	R_1	0.097	0.125	0.141	0.153	0.156		
	R_2	0.099	0.133	0.147	0.161	0.165		
	R_3	0.117	0.160	0.177	0.194	0.200		
	B	0.87(1)	1.55(1)	1.91(1)	2.29(1)	2.42(2)		
$T_2(o)$	R_1	0.096	0.132	0.145	0.159	0.164	0.164	0.169
	R_2	0.104	0.135	0.152	0.168	0.174	0.177	0.199
	R_3	0.114	0.153	0.171	0.185	0.187	0.191	0.254
	B	0.87(1)	1.56(1)	1.93(1)	2.31(1)	2.43(2)	2.49(1)	3.5(1)
$T_2(m)$	R_1	0.096	0.128	0.141	0.156	0.161		
	R_2	0.102	0.142	0.158	0.173	0.178		
	R_3	0.112	0.150	0.167	0.181	0.186		
	B	0.85(1)	1.55(1)	1.91(1)	2.29(1)	2.42(2)		
O_{A1}	R_1	0.119	0.149	0.157	0.174	0.173	0.180	0.170
	R_2	0.144	0.198	0.224	0.247	0.253	0.249	0.255
	R_3	0.170	0.232	0.253	0.273	0.281	0.284	0.295
	B	1.68(3)	3.03(4)	3.66(5)	4.37(6)	4.55(6)	4.62(7)	4.8(5)
O_{A2}	R_1	0.116	0.144	0.160	0.174	0.183	0.180	0.181
	R_2	0.123	0.166	0.177	0.190	0.194	0.197	0.252
	R_3	0.155	0.205	0.225	0.247	0.251	0.258	0.302
	B	1.39(3)	2.37(4)	2.83(4)	3.35(4)	3.54(5)	3.62(5)	4.9(5)
$O_B(o)$	R_1	0.121	0.155	0.168	0.178	0.181	0.176	0.172
	R_2	0.144	0.208	0.239	0.264	0.272	0.279	0.298
	R_3	0.173	0.235	0.256	0.286	0.299	0.306	0.332
	B	1.72(3)	3.22(5)	3.98(5)	4.82(6)	5116(7)	5.34(6)	6.0(6)
$O_B(m)$	R_1	0.114	0.151	0.165	0.173	0.176		
	R_2	0.168	0.235	0.252	0.269	0.269		
	R_3	0.180	0.243	0.270	0.295	0.300		
	B	1.93(3)	3.61(5)	4.30(6)	4.98(6)	5.10(7)		
$O_C(o)$	R_1	0.124	0.160	0.172	0.188	0.187	0.187	0.201
	R_2	0.139	0.186	0.205	0.221	0.230	0.236	0.270
	R_3	0.155	0.210	0.237	0.258	0.265	0.274	0.341
	B	1.54(3)	2.75(4)	3.37(4)	3.96(5)	4.15(5)	4.36(4)	6.0(5)
$O_C(m)$	R_1	0.121	0.152	0.167	0.182	0.184		
	R_2	0.136	0.186	0.205	0.224	0.231		
	R_3	0.166	0.22	0.244	0.264	0.266		
	B	1.60(3)	2.82(4)	3.41(4)	4.03(5)	4.17(5)		
$O_D(o)$	R_1	0.117	0.147	0.159	0.175	0.178	0.174	0.198
	R_2	0.138	0.197	0.225	0.249	0.259	0.268	0.276
	R_3	0.157	0.224	0.247	0.271	0.276	0.283	0.314
	B	1.51(3)	2.90(5)	3.60(4)	4.36(6)	4.61(6)	4.80(5)	5.6(4)
$O_D(m)$	R_1	0.111	0.146	0.161	0.171	0.175		
	R_2	0.151	0.212	0.234	0.255	0.262		
	R_3	0.172	0.234	0.254	0.278	0.276		
	B	1.71(3)	3.18(5)	3.82(5)	4.51(6)	4.63(6)		
Na_1^*	R_1	0.137	0.202	0.225	0.233	0.229	0.247	0.298
	R_2	0.173	0.284	0.325	0.377	0.381	0.370	0.460
	R_3	0.313	0.361	0.372	0.415	0.430	0.428	0.504
	B	3.87	6.63	7.75	9.70	10.08	10.04	14.74
Na_2^*	R_1	0.123	0.179	0.208	0.218	0.224		
	R_2	0.166	0.264	0.324	0.386	0.374		
	R_3	0.273	0.343	0.364	0.424	0.454		
	B	3.09	5.79	7.39	9.89	10.43		

* 2 Na Model

this progressive change toward monoclinic symmetry is the displacive transformation referred to as "U" by Thompson *et al.* (1974) and also Helgeson *et al.*'s (1978) second lambda transition. The fact that obliquity changes much more in high albite than in low albite, as temperature is raised, may explain the calorimetric results of Holm and Kleppa (1968), who found that at 698°C the enthalpy difference between analbite and low albite is significantly greater than the corresponding difference at 25°C.

Na-coordination in monalbite and low albite

In monalbite (see below), the aluminosilicate cage forms a fairly regular 9-fold coordination polyhedron about the Na atom, which, along with O_{A2}, lies on the mirror plane. The remaining eight oxygen atoms occur in mirror-related pairs representing a distorted cube. The two longest bonds in monalbite are Na–O_C bonds (3.133A, Table 7). In low albite at 970°C the

Table 6. High albite (Tiburon) and monalbite (Amelia): Na–O and T–O bond lengths (A) as a function of temperature (with standard deviations in parentheses)

	25°C	500°C	750°C	980°C	1040°C	980°C M	1060°C M
$Na-O_{A1}$	2.606(3)	2.682(4)	2.714(4)	2.744(5)	2.752(5)	2.755(4)	2.764(11)
$-O_{A1}$	2.703(3)	2.720(4)	2.736(4)	2.746(5)	2.748(5)	2.755(4)	2.764(11)
$-O_{A2}$	2.341(2)	2.380(3)	2.401(3)	2.425(4)	2.431(4)	2.436(5)	2.505(18)
$-O_{B}(o)$	2.517(2)	2.637(4)	2.727(5)	2.854(5)	2.903(5)	2.931(5)	2.946(11)
$-O_{B}(m)$	3.184(4)	3.165(5)	3.114(5)	3.007(5)	2.950(5)	2.931(5)	2.946(11)
$-O_{C}(o)$	3.370(3)	3.284(4)	3.243(4)	3.174(5)	3.142(5)	3.133(3)	3.156(11)
$-O_{C}(m)$	2.914(3)	3.000(4)	3.029(4)	3.097(5)	3.124(5)	3.133(3)	3.156(11)
$-O_{D}(o)$	2.496(2)	2.597(4)	2.663(4)	2.771(5)	2.822(5)	2.832(6)	2.825(14)
$-O_{D}(m)$	3.135(4)	3.029(5)	2.983(5)	2.895(5)	2.852(5)	2.832(6)	2.825(14)
	2.807	2.833	2.846	2.857	2.858	2.817	2.851
$T_1(o)-O_A$	1.646(2)	1.648(3)	1.646(2)	1.644(3)	1.651(3)	1.648(1)	1.642(3)
$-O_B$	1.644(2)	1.643(3)	1.637(2)	1.634(3)	1.631(3)	1.636(2)	1.638(12)
$-O_C$	1.647(2)	1.644(3)	1.642(2)	1.642(3)	1.641(3)	1.650(2)	1.654(4)
$-O_D$	1.657(2)	1.657(3)	1.657(2)	1.654(3)	1.652(3)	1.654(2)	1.645(3)
	1.649	1.648	1.646	1.644	1.644	1.647	1.645
$T_1(m)-O_A$	1.655(2)	1.652(3)	1.651(2)	1.652(3)	1.650(3)		
$-O_B$	1.628(2)	1.625(3)	1.624(2)	1.625(3)	1.628(3)		
$-O_C$	1.648(2)	1.642(3)	1.645(2)	1.641(3)	1.642(3)		
$-O_D$	1.635(2)	1.643(3)	1.644(2)	1.646(3)	1.651(3)		
	1.642	1.641	1.641	1.641	1.643		
$T_2(o)-O_A$	1.653(2)	1.654(2)	1.654(2)	1.648(2)	1.648(2)	1.653(1)	1.645(5)
$-O_B$	1.644(2)	1.641(3)	1.636(3)	1.632(3)	1.634(3)	1.627(2)	1.617(12)
$-O_C$	1.635(2)	1.642(3)	1.640(2)	1.639(3)	1.640(3)	1.632(2)	1.616(8)
$-O_D$	1.629(2)	1.632(3)	1.633(2)	1.633(3)	1.637(3)	1.635(2)	1.638(4)
	1.640	1.643	1.641	1.638	1.640	1.637	1.629
$T_2(m)-O_A$	1.653(2)	1.653(2)	1.651(2)	1.652(2)	1.651(3)		
$-O_B$	1.629(2)	1.627(3)	1.625(3)	1.631(3)	1.632(3)		
$-O_C$	1.639(2)	1.643(2)	1.641(2)	1.638(3)	1.640(3)		
$-O_D$	1.646(2)	1.642(3)	1.640(2)	1.635(3)	1.636(3)		
	1.642	1.641	1.639	1.639	1.640		

M=monoclinic

crystal structure does not closely approach monoclinic symmetry (α = 93.33° and γ = 87.56°; Winter *et al.*, 1977). As a result, the aluminosilicate cage about Na in low albite is slightly more distorted than in monalbite at equivalent temperatures. In low albite the $Na-O_B(m)$ and $Na-O_C(m)$ bond lengths are 3.402 and 3.291A respectively. As the $Na-T_2(m)$ distance is 3.330A, these two oxygen atoms may be considered out of the Na coordination sphere. The average difference in Na–O bond lengths between low albite and monalbite at 970–980°C is 0.19A, and the maximum difference is 0.47A. O–Na–O angles vary less than 8°, and the average is 4° variation.

Na anisotropy in high albite

Ferguson *et al.* (1958) recognized the anisotropy of the electron-density distribution of the sodium atom in both high and low albite. The elongated electron-

Table 7. High albite (Tiburon) and monalbite (Amelia): O-T-O and T-O-T bond angles (°) as a function of temperature (with standard deviations in parentheses)

		25°C	500°C	750°C	980°C	1040°C	980°C M	1060°C M
T_1(o)	ATB	104.7(1)	104.8(2)	105.1(1)	105.0(2)	104.8(2)	105.2(1)	105.4(3)
	ATC	114.8(1)	113.9(1)	113.5(1)	113.6(2)	113.7(2)	113.3(1)	112.3(3)
	ATD	104.9(1)	105.5(1)	105.7(1)	105.9(2)	105.7(2)	105.3(1)	105.8(3)
	BTC	110.7(1)	111.4(1)	111.4(1)	111.5(2)	111.7(2)	111.7(2)	112.1(6)
	BTD	111.9(1)	111.6(2)	111.5(1)	111.7(2)	111.7(2)	111.8(2)	112.1(4)
	CTD	109.6(1)	109.4(1)	109.4(1)	109.0(2)	109.1(2)	109.4(1)	108.9(4)
T_1(m)	ATB	106.4(1)	106.0(2)	106.1(2)	105.5(2)	105.2(2)		
	ATC	112.1(1)	112.5(1)	112.9(1)	113.3(2)	113.6(2)		
	ATD	106.0(1)	105.9(2)	105.8(1)	105.7(2)	105.4(2)		
	BTC	111.1(1)	111.0(2)	110.9(1)	111.3(2)	111.4(2)		
	BTD	111.7(1)	112.1(2)	112.0(2)	111.9(2)	111.7(2)		
	CTD	109.4(1)	109.3(1)	109.1(1)	108.9(2)	109.3(2)		
T_2(o)	ATB	108.3(1)	108.5(1)	108.9(1)	109.1(2)	109.0(2)	109.1(2)	108.8(5)
	ATC	105.3(1)	105.2(1)	105.1(1)	105.5(1)	105.4(1)	105.3(1)	106.4(5)
	ATD	108.4(1)	108.3(1)	108.3(1)	108.2(1)	107.9(2)	107.9(2)	107.5(3)
	BTC	111.3(1)	110.8(2)	110.9(1)	110.5(2)	110.8(2)	110.5(2)	109.7(4)
	BTD	110.9(1)	111.4(2)	111.1(1)	111.1(2)	111.2(2)	111.5(2)	111.6(5)
	CTD	112.4(1)	112.3(2)	112.2(1)	112.1(2)	112.2(2)	112.3(2)	112.7(5)
T_2(m)	ATB	110.6(1)	110.3(2)	110.1(1)	109.5(2)	109.1(2)		
	ATC	106.9(1)	106.3(1)	106.0(1)	105.9(1)	105.7(1)		
	ATD	107.9(1)	108.0(1)	108.0(1)	107.9(1)	107.9(2)		
	BTC	110.1(1)	110.2(2)	110.2(2)	110.5(2)	110.7(2)		
	BTD	110.0(1)	110.2(2)	110.5(2)	110.9(2)	111.1(2)		
	CTD	111.3(1)	111.8(1)	111.9(1)	112.0(2)	112.1(2)		
T1-OA1-T1		143.2(1)	144.0(2)	144.3(2)	144.3(2)	144.0(2)	144.2(3)	145.4(4)
T2-OA2-T2		129.7(1)	130.5(1)	131.2(2)	132.0(2)	132.1(2)	132.0(2)	134.2(7)
T1-OBo-T2		141.4(1)	143.9(2)	146.6(2)	149.3(2)	150.3(2)	151.2(2)	151.1(4)
T1-OBm-T2		158.8(1)	156.9(2)	155.8(2)	152.8(2)	151.5(2)	151.2(2)	151.1(4)
T1-OCo-T2		130.4(1)	131.7(2)	132.4(2)	133.3(2)	133.5(2)	133.6(2)	134.5(6)
T1-OCm-T2		134.6(1)	134.4(2)	134.0(2)	134.0(2)	133.5(2)	133.6(2)	134.5(6)
T1-ODo-T2		135.3(1)	137.2(2)	138.2(2)	140.6(2)	141.3(2)	137.4(2)	141.2(5)
T1-ODm-T2		149.5(1)	147.0(2)	145.6(2)	143.6(2)	142.1(2)	137.4(2)	

M-monoclinic

density peak in low albite could be either a result of the anisotropic thermal motion or the random occupancy by the Na atom of one of two positions approximately 0.1A apart. High albite exhibited even greater anisotropy and required four collinear isotropic Na quarter-atoms to express it.

High-temperature studies of low albite have demonstrated that the isotropic equivalent temperature factor (B) of Na extrapolates to zero at 0°K (Winter *et al.*, 1977). This indicates that there is a single nonvibrating Na atom at this temperature and implies that the large observed sodium anisotropy at room

Table 9. High albite (Tiburon): "obliquity" as a function of temperature

	25°C			500°C			750°C			980°C			1040°C		
	Δx	Δy	Δz	Δx	Δy	Δz	Δx	Δy	Δz	Δx	Δy	Δz	Δx	Δy	Δz
T_1	4.2	20.5	14.2	2.8	14.9	10.4	2.2	10.9	7.5	0.8	4.4	2.8	0.3	0.6	0.0
T_2	5.5	14.4	33.5	3.3	10.2	24.1	2.1	7.5	17.5	0.8	3.0	6.6	0.2	0.8	1.8
O_{A1}	5.3		15.6	4.2		11.3	2.6		8.4	0.7		3.0	-0.1		1.1
O_{A2}		9.2			6.7			5.1			1.8			0.4	
O_B	2.6	44.2	46.5	0.7	32.0	34.7	0.6	23.1	25.0	-0.2	9.0	9.4	-0.1	2.5	3.0
O_C	5.8	22.2	58.9	2.9	15.8	42.3	1.3	11.9	30.2	0.5	4.5	11.9	-0.2	1.4	3.2
O_D	7.8	20.4	38.8	3.9	14.6	27.4	2.8	11.6	19.8	1.3	4.8	7.4	0.5	1.2	1.9

Δx=the difference in the x coordinates of atom pairs related by mirror symmetry in the monoclinic case i.e. $[x_o-x_m]$ Likewise, $\Delta z=[z_o-z_m]$ and $\Delta y=[(1-y_0)-y_m]$. A negative value indicates that the calculated value has passed through zero.

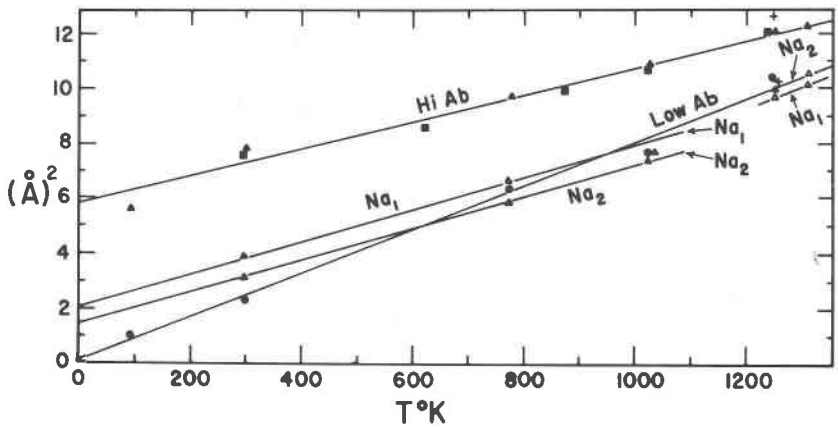

Fig. 7. Isotropic equivalent temperature factor (B) for the Na atom in high albite, low albite, and monalbite *vs.* temperature. Dots represent the data for low albite and triangles represent the data for high albite. The two-Na model is shown as open triangles. Squares represent the high albite data of Prewitt *et al.* (1976). Monalbite is indicated as plus signs.

temperature and above is the result of highly anisotropic thermal motion about a single node. Similar plots of B *vs.* absolute temperature for the sodium atom in high albite from this study and that of Prewitt *et al.* (1976) are shown in Figure 7. The data for low albite (Winter *et al.*, 1977) are included for reference. Unlike the behavior of Na in low albite, the B value in high albite, extrapolated to 0°K, is 5.85A², which is equivalent to $\bar{u}$ = 0.272A, or two stationary atom centers separated by 0.272A at 0°K. As deduced by Prewitt *et al.* (1976), some form of static spatial disorder must exist in high albite.

The concept of spatial disorder with respect to feldspars has been discussed by Megaw (1959, 1960a,b,c, 1962), Williams and Megaw (1964), and Ribbe *et al.* (1969). Multiple Na positions are most often attributed to domain textures, each domain having a single unique Na site. The resulting albite structure would then be an average of these domains. The two most prevalent models for such domains are: (1) a four-Na model or "quadripartite" cell similar to the anorthite structure, containing four albite-like subcells differing in the distribution of Al and Si in the four T sites, and (2) a two-Na model such as unit-cell-scale albite twinning or a doubled unit cell with c = 14A. A doubled cell must be separated by fault boundaries with a slip of one-half of the repeat distance in order to eliminate superlattice reflections, which have not been observed in albite. A third possible cause of the observed diffuse electron-density distribution would be the existence of two or more positions of low potential energy within the large aluminosilicate cage, with Na atoms randomly occupying them or oscillating between them. However, if such positions are the result of the Al/Si distribution in the cage framework, this explanation of the spatial disorder is no different from the previous ones. That the multiple low-potential-energy positions do not result from the shape of the aluminosilicate cage in high albite is clear from the fact that low albite, with a very similar cage, does not show spatial disorder.

The shape of the thermal ellipsoid in high albite (Table 5) is much more prolate than that of low albite at room temperature. However, as temperature is raised, the Na ellipsoid in high albite quickly becomes oblate as R_3 (the long axis of the ellipsoid) decreases above 500°C. Although this behavior is quite different from low albite, the orientations of the three axes of the Na ellipsoid are remarkably similar for both low and high albite.

A difference-Fourier map of an isotropic approximation of the Na position using the 1040°C data revealed three positive peaks in a triangular arrangement in the (100) plane about the Na center. As the vibration of the Na atom is known to be highly anisotropic, this arrangement indicated two anisotropic Na atoms overlapping slightly at one end in an inverted "V" shape. Such a relationship mimicked the (010) mirror equivalence of albite twinning. Subsequent refinement of two equally-distributed anisotropic split-Na atoms reduced the R factors compared to the one-Na model at all temperatures [although less so at high temperatures (Table 1)]. The 2-Na model is significantly better than the 1-Na model at 25, 500, 750, and 980°C at the 100 percent significance level and at 1040°C at 50 percent significance level (Hamilton, 1964).

A model using fine domains based on albite twinning seemed promising, particularly in view of the fact that high albite is often twinned according to the

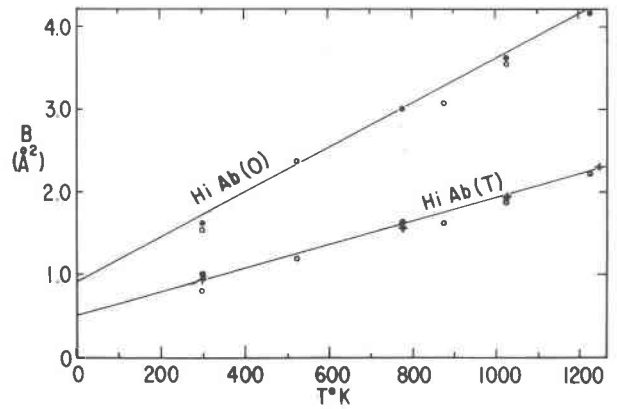

Fig. 8. Average isotropic equivalent temperature factors (B) for T and O atoms for high albite *vs.* temperature. Dots and crosses represent the data for O and T atoms respectively. Open circles represent the data of Prewitt *et al.* (1976).

albite law (Okamura and Ghose, 1975a; Prewitt *et al.*, 1976). The converging values of B for high and low albite at high temperatures (Fig. 7) are consistent with twinned domains. At higher temperatures the differences between the domains become less and the cause of the spatial disorder diminishes. But if the differences are the result of albite twinning only, these values should converge to a single value at about 1300°K with the attainment of monoclinic symmetry, which they fail to do. The positions and thermal parameters of the two Na half-atoms are included in Tables 4 and 5. As we noticed in the 1040°C difference-Fourier map, the two Na positions are nearly mirror-related. As the temperature is raised, the distance separating them progressively decreases from 0.704A at 25° to 0.526A at 1040°C in high albite, and from 0.544A at 980° to 0.441A at 1060°C in monalbite; monoclinic symmetry is approached, and Na moves toward the mirror plane. As the half-atoms become closer, the overlap of the electron clouds increases and the single-atom model becomes a better fit. This fact explains the diminished lowering of R factor using the two-Na model at higher temperatures. However, at room temperature, the long axes of the ellipsoids of the two half-atoms are parallel to each other as well as to the direction of separation of the atom centers, and are no longer mirror images of one another. The difference in z coordinates for the two half-atoms is too large at low temperatures to be a result of albite twinning. Furthermore, a difference Fourier synthesis of monalbite for the 2-Na model at 980°C shows a small positive residual electron density on the mirror plane.

The average B values for the T and O atoms, when plotted against T in Kelvins (Fig. 8) extrapolate to B = 0.51 and 0.93A² ($\bar{u}$ = 0.081 and 0.108A) respectively at 0°K. These values also indicate spatial disorder, but are substantially lower than the corresponding value for the single Na atom. Superposition of unit cells measured at room temperature related by the albite twin law results in larger spatial disorder with respect to T and O atoms (~0.4A) than is observed. A model based on twinned domains is thus considered unlikely, especially at low temperatures. A two-Na model based on a double repeat distance with different Al distributions or on two low-potential-energy Na positions is still possible. When B *vs.* absolute temperature is plotted for each of the half-atoms in Figure 7, extrapolated values of B = 2.20 and 1.35A² ($\bar{u}$ = 0.167 and 0.131A) result for Na_1 and Na_2, respectively. These values reduce the residual spatial disorder by 40–50 percent, but do not eliminate it. The B *vs.* T data for the two-Na model show an interesting phenomenon (Fig. 7): between 750 and 980°C (1023 and 1253 K) the values of B for the half-atoms show a discontinuous increase, and their relative sizes reverse. A relationship between this change and the triclinic/monoclinic transition for analbite, which also occurs within this temperature interval, is possible. However, no other discontinuities were observed.

An alternative model using four isotropic Na positions (Ribbe *et al.*, 1969) resulted in little or no reduction in R factors at high temperatures in the high albite study of Prewitt *et al.* (1976); plots of B *vs.* T (K) for four Na quarter-atoms extrapolate to a B value of ~1A² ($\bar{u}$ = 0.113A). The four-Na model thus results in a further reduction of the spatial disorder of only about 10 percent, and also fails to eliminate it.

If we assume that the complete Al/Si disorder is the basis for the four-Na model, there is no compelling reason to believe that each tetrahedral ring must contain three Si atoms and one Al atom. Other configurations are definitely possible. Some rings may have four Si atoms and some two Si and two Al atoms. The aluminum-avoidance rule only requires that the two Al atoms in such a ring cannot be neighbors. Thus, there are far more than the four previously-assumed topochemical configurations and, as a result, more than four Na atom positions. This fact explains the residual spatial disorder at 0°K in the four-Na model. This view is consistent with the "lattice" energy calculation of Brown and Fenn (1978) for high albite at 24°C, which shows a broad minimum potential-energy well slightly elongated parallel to c, with no indication of either two or four minima.

The drastic change in the shape of the Na electron-density distribution from highly prolate to highly oblate with increasing temperature reflects the distortion of the aluminosilicate cage surrounding the Na atom. At high values of α (low temperature) the cage is more distorted, and the long Na vibration direction is nearly parallel to the long diagonal of the cage (Fig. 9a). As α decreases toward 90° with increasing temperature, the cage becomes more cubic and Na vibrates randomly in a plane normal to the short Na–O_{A2} bond (Fig. 9b). Thus, in high albite, the changes in Na behavior reflect the approach to monoclinic symmetry.

Monalbite and the triclinic → monoclinic phase transformation

Although Tuttle and Bowen (1950) first attempted an investigation of a possible triclinic → monoclinic phase transformation by means of differential heating curves, they found no evidence for a heat effect. MacKenzie (1952), using powder-diffraction data, showed that $(2\theta_{111} - 2\theta_{1\bar{1}1})$ could be used as a triclinic indicator in synthetic Na-rich feldspars, and that this indicator decreased in magnitude as temperature increased, the (111) and (1$\bar{1}$1) reflections becoming a single monoclinic peak at about 1180°C (extrapolated) for pure high albite. He also showed that values of the indicator were also a function of the temperature of synthesis, as well as any subsequent heat treatment. Laves (1952, 1960) proposed that the effects of higher synthesis and annealing temperatures were to increase the degree of Al/Si disorder. Once the disorder became complete, the transition to the monoclinic form would be possible. Laves placed this inversion temperature (T_c) at 980°C, while MacKenzie and Smith (1961) placed it at 950°C. Grundy *et al.* (1967), using the precession technique, found that a synthetic albite became monoclinic at about 930°C. Kroll (1971) placed T_c at 980°C based on powder data, while Okamura and Ghose (1975a), also using the precession method, placed it at 930°C.

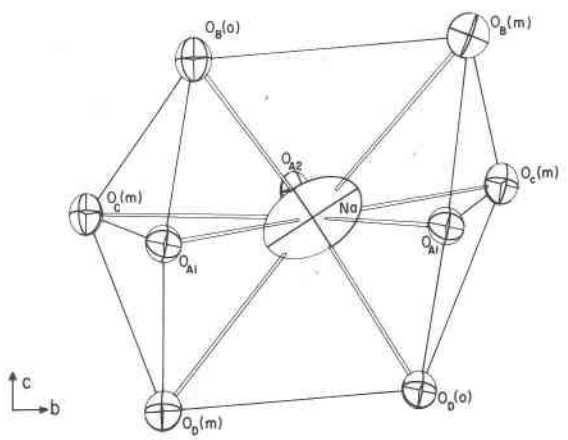

Fig. 9a. Na atom coordination in high albite at 25°C.

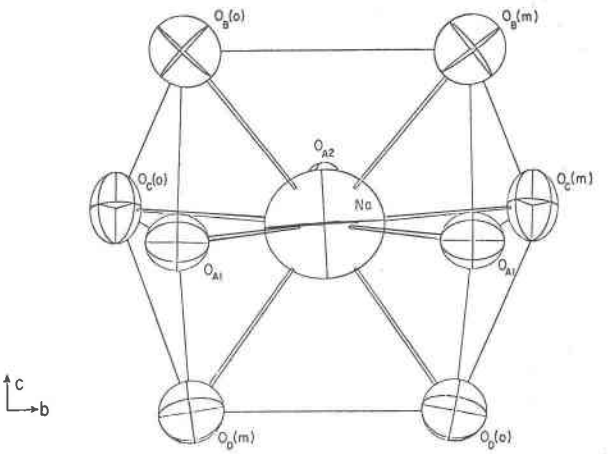

Fig. 9b. Na atom coordination in high albite at 1040°C.

Based on three-dimensional crystal-structure analyses of high albite at elevated temperatures, Prewitt *et al.* (1976) found that monoclinic symmetry was closely approached but not quite attained at or below 1105°C. The high sensitivity of the diffractometer data cast some doubt on the previous results. Our investigation on the annealed Tiburon albite confirmed in part the findings of Prewitt *et al.* (1976). The structure, although nearly monoclinic at 1040°C, indeed did not become monoclinic within the temperature range of study. A calculation of monoclinic indicators such as "obliquity" (Fig. 5) and the symmetry relations of Na–O bond lengths (Fig. 6) extrapolates to monoclinic values in the range 1050–1073°C. On the other hand, our crystal-structure analysis of the Amelia sample used by Duba and Piwinskii (1974) and Okamura and Ghose (1975b) showed it was clearly monoclinic at 980°C.

The atomic parameters and interatomic distances of the monoclinic Amelia albite at 980°C closely match the corresponding extrapolated monoclinic values of the Tiburon sample (Fig. 6, Table 4). We therefore conclude that no perceptible discontinuities accompany the triclinic/monoclinic transition. Small shifts in the positions of the atoms occur in monalbite between 980 and 1060°C, especially of the O_{A2} atom closest to Na.

"Obliquity" values and the Na–O bond distance relationships for the 1105°C data of Prewitt *et al.*

(1976) indicate monoclinic symmetry was attained at 1105°C.

If two different albite samples studied did not become monoclinic below 1040°C and one did below 980°C, what factors control the temperature at which this transition takes place? The chemical compositions and thermal histories of the three samples are:

Tiburon albite	$Or_{0.25}Ab_{99.75}An_0$
	Annealed at 1080°C for 60 days
Amelia albite	$Or_{0.6}Ab_{99.3}An_{0.1}$
	Annealed at 1080°C for 21 days+ at 1100°C for 50 days+ at 1111°C for 62 days
Synthetic albite	$Or_{0.5}Ab_{98.3}An_{1.2}$
	Synthesized at 700°C and annealed at 1060°C for 40 days

Compositional differences do not appear to explain the discrepancy, since the Amelia albite, which did become monoclinic, is of a composition intermediate between the two samples which did not. The reason for the different transition temperatures must lie with the thermal histories and, therefore, the degree of Al/Si disorder specific to the various samples, as Laves (1952, 1960) postulated.

The Amelia sample received from Duba and Piwinskii (1974) had glassy rinds, indicating that partial melting at temperatures near the melting temperature of 1118°C was attained during the annealing period. There is a correlation between the higher temperature (and time) of annealing and the lower T_c. This agrees with the results of MacKenzie (1952) and Kroll (1971) that lower hydrothermal synthesis temperatures of albites resulted in higher temperatures for the monoclinic inversion.

An albite which is topochemically monoclinic inverts to the monoclinic structural form in the vicinity of 930°C, at which point the thermal energy of the aluminosilicate framework becomes capable of overcoming the collapse about the small Na atom. Small amounts of residual Al/Si order destroy the monoclinic topochemical symmetry; hence, greater amounts of thermal energy are required to overcome the slight deviations from monoclinic topochemistry created by the non-random Al–Si distribution. It is also possible that the small amounts of residual Al/Si order are great enough to profoundly impede the attainment of true monoclinic symmetry. The asymptotic approach of α to 90° and the crossing of the 90° value by γ with increasing temperature shown in Figure 2 may be real, and slight further disordering or larger thermal overstepping may be required before true monoclinic symmetry can be attained.

The Al occupancy of a given T site is usually considered to be a linear function of the mean tetrahedral bond length (Smith, 1954; Smith and Bailey, 1963). From this assumption, Ribbe and Gibbs (1969) derived an equation for calculating the Al occupancy of the T sites in feldspars. Because the Amelia specimen becomes finely twinned below the inversion temperature, a room-temperature structure analysis is not available and the calculation of Al occupancy is hindered. Since the T–O bond lengths vary notoriously little with temperature, a comparison of the mean T–O bond lengths for the T sites in the three samples may be made at 980°C (interpolating the data of Prewitt *et al.*, 1976) and the relative Al contents compared:

	Tiburon		Synthetic		Amelia	
	mean T–O	*%Al*	*mean T–O*	*%Al*	*mean T–O*	*%Al*
$T_1(o)$	1.644(3)	0.26	1.645(3)	0.26	1.647(2)	0.28
$T_1(m)$	1.641(3)	0.24	1.641(3)	0.24	1.647(2)	0.28
$T_2(o)$	1.638(3)	0.22	1.638(3)	0.22	1.637(2)	0.21
$T_3(m)$	1.639(3)	0.22	1.635(3)	0.20	1.637(2)	0.21
		0.94		0.92		0.98

It would appear from these data that the monoclinic Amelia albite is less disordered than the other two specimens. However, the differences are of a magnitude commensurate with the uncertainties in the measurements, and probably those inherent in the method of determining the Al occupancies as well. The method assumes that all four T sites are structurally identical in size, and variations in mean T–O bond lengths are strictly a result of relative differences in Al/Si occupancy. It is clear that the four T sites are structurally different and may have intrinsically different T–O bond lengths. These intrinsic differences must be known before accurate calculations of the Al occupancy from T–O bond lengths can be attempted. Alternative methods of measuring the degree of order such as the *b–c* plot (Orville, 1967) and α^*–γ^* plot (MacKenzie and Smith, 1962) are equally inadequate in detecting the minute differences. We therefore agree with Grundy *et al.* (1967) and Prewitt *et al.* (1976) that it is impossible to determine the exact structural state of high albite on the basis of room-temperature lattice parameters. Furthermore, it is currently impossible to fully characterize albite on the basis of bond distances. The minute

differences in the degree of Al/Si order which are difficult to detect have a profound effect on T_c.

Acknowledgments

We are indebted to Professor Bernard W. Evans, University of Washington for the albite sample from Tiburon, and Drs. A. Duba and A. J. Piwinskii, Lawrence Livermore Laboratory, Livermore, California, for the heat-treated Amelia albite sample. This paper has benefited from critical reviews by Dr. H. Kroll, University of Münster, Germany and Professors F. Laves, Eidg. Technische Hochschule, Zürich, C. T. Prewitt, State University of New York at Stony Brook, G. E. Brown, Stanford University, and B. W. Evans, J. A. Vance and I. S. McCallum at the University of Washington. This research has been supported by NASA grant NGR 48-002-149 and NSF (Geochemistry) grants EAR 76-13373 (S.G.) and EAR 75-14904 (B. W. Evans).

References

Brown, G. E. and P. M. Fenn (1978) Structure energies of the alkali feldspars. *Phys. Chem. Minerals* (in press).

Cromer, D. T. and D. Liberman (1970) Calculation of anomalous scattering factors for X-rays. *J. Chem. Phys., 53,* 1891–1898.

——— and J. B. Mann (1968) X-Ray scattering factors computed from numerical Hartree-Fock wave functions. *Acta Crystallogr., A24,* 321–324.

Duba, A. and A. J. Piwinskii (1974) Electrical conductivity of albite. *Trans. Am. Geophys. Union, 55,* 470.

Ferguson, R. B., R. J. Traill and W. H. Taylor (1958) The crystal structures of low-temperature and high-temperature albites. *Acta Crystallogr., 11,* 331–348.

Finger, L. W. (1969) Determination of cation distribution by least-squares refinement of single-crystal X-ray data. *Carnegie Inst. Wash. Year Book, 67,* 216–217.

Grundy, H. D., W. L. Brown and W. L. MacKenzie (1967) On the existence of monoclinic $NaAlSi_3O_8$ at elevated temperatures. *Mineral. Mag., 36,* 83–88.

Hamilton, W. C. (1964) *Statistics in Physical Science.* Ronald Press, New York.

Helgeson, H. C., J. M. Delaney, H. W. Nesbitt and D. K. Bird (1978) Summary and critique of the thermodynamic properties of rock-forming minerals. *Am. J. Sci.* (in press).

Holm, J. L. and O. J. Kleppa (1968) Thermodynamics of the disordering process in albite. *Am. Mineral., 53,* 123–133.

Kroll, H. (1971) Feldspäte im System $KAlSi_3O_8$–$NaAlSi_3O_8$–$CaAl_2Si_2O_8$–Al,Si Verteilung und Gitterparameter, Phasen-Transformationen und Chemismus. *Inaug.-Diss. der Westfälischen Wilhelms-Universität in Münster.*

——— (1973) Estimation of the Al,Si distribution of feldspars from the lattice translations Tr[110] and Tr[1$\bar{1}$0]. I. Alkali feldspars. *Contrib. Mineral. Petrol., 39,* 141–156.

Laves, F. (1952) Phase relations of the alkali feldspars II. The stable and pseudo-stable phase relations of the alkali feldspar system. *J. Geol., 60,* 549–574.

——— (1960) Al/Si-Verteilungen, Phasen-transformationen und Namen der Alkalifeldspäte. *Z. Kristallogr., 113,* 265–296.

MacKenzie, W. S. (1952) The effect of temperature on the symmetry of high-temperature soda-rich feldspars. *Am. J. Sci., Bowen Vol.,* 319–342.

——— and J. V. Smith (1961) Experimental and geological evidence for the stability of alkali feldspars. *Cursillos y Conferencias Inst. "Lucas Mallada" 8,* 53–69.

Megaw, H. D. (1959) Order and disorder in the feldspars. *Mineral. Mag., 32,* 226–241.

——— (1960a) Order and disorder I. Theory of stacking faults and diffraction maxima. *Proc. R. Soc. Lond., Ser. A, 259,* 59–78.

——— (1960b) Order and disorder II. Theory of diffraction effects in the intermediate plagioclase feldspars. *Proc. R. Soc. Lond., Ser. A, 259,* 159–183.

——— (1960c) Order and disorder III. The structure of the intermediate plagioclase feldspars. *Proc. R. Soc. Lond., Ser. A, 259,* 184–202.

——— (1962) Order and disorder in feldspars. *Norsk Geol. Tidsskr., 42,* 104–137.

Ohashi, Y. and L. W. Finger (1973) Lattice deformations in feldspars. *Carnegie Inst. Wash. Year Book, 72,* 569–573.

Okamura, F. P. and S. Ghose (1975a) Analbite→monalbite transition in a heat-treated twinned Amelia albite. *Contrib. Mineral. Petrol., 50,* 211–216.

——— and ——— (1975b) Crystal structure of monalbite at 980°C (abstr.). *Geol. Soc. Am. Abstracts with Programs, 7,* 1218.

Orville, P. M. (1967) Unit-cell parameters of the microcline–low albite and the sanidine–high albite solid solution series. *Am. Mineral., 52,* 55–86.

Prewitt, C. T., S. Sueno and J. J. Papike (1976) The crystal structures of high albite and monalbite at high temperatures. *Am. Mineral., 61,* 1213–1225.

Ribbe, P. H. and G. V. Gibbs (1969) Statistical analysis and discussion of mean Al/Si–O bond distances and the aluminum content of tetrahedra in feldspars. *Am. Mineral., 54,* 85–94.

———, H. D. Megaw, W. H. Taylor, R. B. Ferguson and R. J. Traill (1969) The albite structures. *Acta Crystallogr., 25B,* 1503–1518.

Smith, J. V. (1954) A review of the Al–O and Si–O distances. *Acta Crystallogr., 7,* 479–483.

——— (1974) *Feldspar Minerals.* Vol. I. Springer-Verlag, New York.

——— and S. W. Bailey (1963) Second review of Al–O and Si–O tetrahedral distances. *Acta Crystallogr., 16,* 801–810.

Stewart, D. B. and P. H. Ribbe (1969) Structural explanation for variations in cell parameters of alkali feldspars with Al/Si ordering. *Am. J. Sci., Schairer Vol., 267A,* 444–462.

Thompson, J. B., D. R. Waldbaum and G. L. Hovis (1974) Thermodynamic properties related to ordering in end-member alkali feldspars. In W. S. MacKenzie and J. Zussman, Eds., *The Feldspars,* Manchester University Press, Manchester.

Tuttle, O. F. and N. L. Bowen (1950) High-temperature albite and contiguous feldspars. *J. Geol., 58,* 572–583.

Willaime, C., W. L. Brown and M. C. Pernaud (1974) On the orientation of the thermal and compositional strain ellipsoids in feldspars. *Am. Mineral., 59,* 457–464.

Williams, P. P. and H. D. Megaw (1964) The crystal structures of high and low albites at −180°C. *Acta Crystallogr., 17,* 882–890.

Winter, J. K., S. Ghose and F. P. Okamura (1977) A high-temperature study of the thermal expansion and the anisotropy of the sodium atom in low albite. *Am. Mineral., 62,* 921–931.

Manuscript received, April 3, 1978;
accepted for publication, September 2, 1978.